Journal of Alloys and Compounds 516 (2012) 85–90

Contents lists available at SciVerse ScienceDirect

Journal of Alloys and Compounds

journal homepage: www.elsevier.com/locate/jallcom

Graphite oxide–TiO_2 nanocomposite and its efficient visible-light-driven photocatalytic hydrogen production

Peng Zeng, Qinggang Zhang, Xungao Zhang, Tianyou Peng*

College of Chemistry and Molecular Science, Wuhan University, Wuhan 430072, China

ARTICLE INFO

Article history:
Received 28 August 2011
Accepted 28 November 2011
Available online 6 December 2011

Keywords:
TiO_2
Graphite oxide
Nanocomposites
Photocatalytic hydrogen production
Visible light

ABSTRACT

Graphite oxide (GO)–TiO_2 nanocomposite was prepared by a facile hydrothermal process and was characterized by X-ray powder diffraction, Transmission electron microscopy, UV–vis diffusion reflectance spectroscopy, X-ray photoelectron spectroscopy, and Raman spectroscopy. TiO_2 particles with average particle size of ~20 nm in the nanocomposites are attached to the surface of GO and/or intercalated into the interlayer of GO. The obtained GO–TiO_2 was used as photocatalyst for H_2 production under visible light ($\lambda \geq 420$ nm) irradiation, and an optimal photocatalytic H_2 production rate of 380 μmol h^{-1} can be obtained over 2 wt% GO–TiO_2. The encouraging results presented here demonstrate that GO can serve as visible-light-driven photocatalyst and photosensitizer to expand the photoresponsive range of TiO_2 to visible light for H_2 production. The possible mechanism for H_2 production was proposed for better understanding the visible-light-driven photocatalytic behaviour of the GO–TiO_2 nanocomposite.

1. Introduction

Carbon nanostructured materials such as fullerene, nanotube and graphene are attracting extensive interest because of their unique and novel properties [1–3]. Graphene characterized as "the thinnest material" is the basic building block of graphitic materials of all dimensionalities [4]. The previous studies on versatile applications primarily relied on the physical or chemical exfoliation of graphite sheets, because large-scale production of single layer graphene has not been achieved up till now. Graphite oxide (GO) produced through a harsh oxidation treatment of graphite sheet is usually used as the starting material in most studies, and then the GO is exposed to either a thermal or mechanical (e.g. ultrasonication) treatment to expand or exfoliate the graphitic layers to obtain graphene [5]. Earlier researches demonstrated that oxidation treatment of graphite could open a bandgap and the GO shows some semiconductive properties, whereas the pristine graphene is semimetal with zero bandgap [6,7].

Photocatalytic H_2 production over heterogeneous photocatalyst is a clean method of generating sustainable hydrogen energy from solar radiation [8]. It is well known that TiO_2 is a promising photocatalyst due to its environmentally friendly, abundant and cost effective advantages. Nevertheless, TiO_2 is a wide bandgap semiconductor (*ca.* 3.2 eV), and could only be excited by UV irradiation, which is approximately 4% effectiveness of the solar radiation. Therefore, developing of photocatalysts that can respond to visible light, which is more than 40% effectiveness of the solar energy, have received much attentions. Various efforts have been attempted to extend the light absorption of TiO_2 to the visible region. For example, TiO_2 doped with different metal or nonmetal elements show a slight shift in the bandgap transition to longer wavelengths [8,9]. The TiO_2–C composites are currently being studied widely in different composites and most of them exhibit effective visible-light-driven photoactivities [10–12]. In our previous study, visible-light-driven photoactivity and enhanced H_2 production efficiency are both achieved from a multi-walled carbon nanotubes (MWCNTs)/TiO_2 nanocomposite [13].

Recently, Yeh and co-workers [14] used GO as photocatalyst for H_2 production. Moreover, it was found that GO–TiO_2 or/and graphene–TiO_2 nanocomposites showed high performances on photodegradation of organic compound under visible light [15–19]. GO can not only expand the photoresponsive range to visible light and enhance the absorbance, but also can serve as photo-generated electron transmitter. Therefore the effective suppression of charge recombination resulting in the improvement of photocatalytic activity can be attained. Nevertheless, GO–TiO_2 nanocomposite has seldom been used in photocatalytic H_2 production under visible light [20]. Herein, GO was directly applied as raw material without further chemical reduction to prepare GO–TiO_2 nanocomposite via a hydrothermal process. The effects of GO contents in nanocomposite on the visible-light-driven photocatalytic H_2 production efficiency are investigated. Steady and enhanced photocatalytic H_2 evolution are obtained over GO–TiO_2 nanocomposite under visible light ($\lambda \geq 420$ nm) irradiation in the presence of triethanolamine

* Corresponding author. Tel.: +86 27 68752237; fax: +86 27 68752237.
E-mail address: typeng@whu.edu.cn (T. Peng).

0925-8388/$ – see front matter © 2011 Elsevier B.V. All rights reserved.
doi:10.1016/j.jallcom.2011.11.140

(TEOA). Moreover, the possible mechanism for H_2 production is proposed based on the present experimental results.

2. Experimental

2.1. Material synthesis

Graphite oxide (GO) was synthesized according to a modified Hummers' method [21]. In detail, 5.0 g graphite powder and 2.5 g $NaNO_3$ were added to 115 mL concentrated H_2SO_4 in an ice-bath, then 15.0 g $KMnO_4$ was gradually added under stirring. The mixture was stirred at 35 °C for 4 h, after that 230 mL distilled water was added, followed by stirring the resultant mixture at 98 °C for 15 min. The suspension was further diluted to 700 mL and stirred for 30 min. The reaction was terminated by adding 12 mL H_2O_2 (35 wt%) under stirring at room temperature. The resulting solid was washed with water and ethanol, and dried at 40 °C overnight.

A typical synthesis process for GO–TiO_2 nanocomposite was as follows: 2.4 g Ti $(SO_4)_2$ was dissolved in 20 mL distilled water (denoted as Solution A). 0.44 g CTAB was dissolved in 20 mL distilled water (denoted as Solution B). Solution A was quickly added into the Solution B under stirring, and then different GO contents were added into the mixture. After further stirring for 30 min, the resultant mixture was transferred into 50 mL autoclave and hydrothermally treated at 100 °C for 72 h. The resulting powder was recovered by centrifugation, washed with water and ethanol. Ion-exchange treatment was performed by mixing the as-synthesized powders with a water and ethanol (molar ratio 1:1) solution of NaCl under stirring at 60 °C overnight. The solid was washed with water and ethanol, and then dried at 60 °C overnight. The as-prepared sample was further calcined at 500 °C in nitrogen for 2 h with a heating rate of 4 °C min^{-1}.

Pt-loading was prepared through a photodeposition procedure as follows: H_2PtCl_6 solution and GO–TiO_2 were added into MeOH aqueous solution (containing 20 vol%) in the photoreaction cell (Pyrex glass), and then irradiated by a 500 W high-pressure Hg-lamp for 2 h under continuous stirring. The nanocomposite was recovered by centrifugation and dried at 60 °C overnight. For comparison, the pristine TiO_2 and graphite–TiO_2 (denoted as G–TiO_2) composite were also hydrothermally prepared under a similar procedure. Moreover, the physical mixture containing the pristine TiO_2 and G or GO was also prepared, and denoted as G + TiO_2 or GO + TiO_2, respectively.

2.2. Material characterization

X-ray powder diffraction (XRD) patterns were obtained on a Bruker D8 advance X-ray diffractometer with Cu Kα radiation (λ = 0.15418 nm) at 40 kV and 100 mA. Raman spectra were obtained by Confocal Raman Microspectroscopy (Renishaw RM-100) with excited wavelength at 514 nm. X-ray photoelectron spectra (XPS) were recorded on a Kratos XSAM800 X-ray photoelectron spectroscope equipped with a standard and monochromatic source (Al Kα) operated at 150 W (15 kV, 10 mA). Field emission scanning electron microscopy (FESEM) images were obtained on a JSM-7400F electron microscope. Transmission electron microscopy (TEM) images were obtained on a LaB6 JEM-2010(HT)-FEF electron microscope. The UV–vis diffuse reflectance absorption spectra (DRS) were recorded by a Cary 5000 UV-Vis-NIR spectrophotometer equipped with an integrating sphere using $BaSO_4$ as a reference.

2.3. Photocatalyst evaluation

The photocatalytic H_2 production reaction was carried out in an outer irradiation-type photoreactor (Pyrex glass) connected to a closed gas-circulation system. A 300 W Xe-lamp (PLSSXE 300, Beijing Trusttech Co. Ltd., China) was applied as the light source. A cut-off filter (Kenko, L-42) was used to obtain the visible-light irradiation (λ ≥ 420 nm). Photocatalyst (100 mg) was added to 100 mL (10 vol% TEOA) solution, and then the suspension was thoroughly degassed to remove air, and irradiated from the top of the reactor system. The photocatalytic H_2 evolution rate was analyzed with an online gas chromatograph (GC, SP-6800A, TCD detector, 5 Å molecular sieve columns and Ar carrier).

The apparent quantum yield (AQY) was measured according to Eq. (1) [9] under the same photocatalytic reaction condition except for the light wavelength of irradiation. The H_2 yields of 1 h photoreaction under different light wavelengths (420, 475, 520, and 550 nm) were measured. The band-pass and cutoff filters and a calibrated Si photodiode (SRC-1000-TC-QZ-N, Oriel, USA) were used in above measurement.

$$\text{AQY}\ (\%) = \frac{\text{the number of reacted electrons}}{\text{the number of incident photons}} \times 100 = \frac{2 \times \text{the number of evolved } H_2 \text{ molecules}}{\text{the number of incident photons}} \times 100 \quad (1)$$

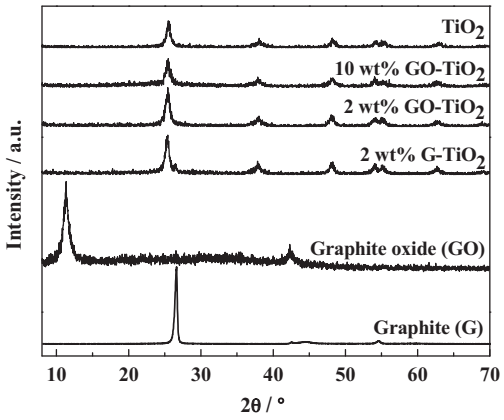

Fig. 1. XRD patterns of graphite (G), graphite oxide (GO), TiO_2, G–TiO_2 and GO–TiO_2 nanocomposites.

3. Results and discussion

3.1. Microstructure analyses

Fig. 1 shows the XRD patterns of graphite (G), GO, G–TiO_2 and GO–TiO_2 containing different GO contents. As can be seen, the diffraction peak at $2\theta = 26.5^\circ$ for graphite disappears, whereas a new sharp diffraction peak at around $2\theta = 11.3^\circ$ can be observed after the oxidation treatment of graphite, indicating the formation of GO [22]. The GO–TiO_2 nanocomposites containing different GO contents show XRD patterns similar to anatase TiO_2 (JCPDS, No. 21-1272) [23] and no diffraction peak of GO can be observed even for 10 wt% GO–TiO_2 due to the disrupted layer-stacking regularity after the hydrothermal process [20].

SEM images of GO and GO–TiO_2 in Fig. 2a and b show that TiO_2 nanoparticles with average particle size of *ca.* 20 nm ranging from 5 to 25 nm mounted on the stacked and wrinkled GO sheets. HRTEM images in Fig. 2c–e indicate that TiO_2 nanoparticles are mounted on the GO sheet surfaces and some particles intercalate between the GO interlayer. The interlayer-spacing of GO is 0.44 nm, which is in agreement with the literature [14]. The well-resolved aligned lattice fringes of TiO_2 with spacing of *ca.* 0.33 nm reveals exactly anatase phase. Energy-dispersive X-ray (EDX) spectrum in Fig. 2f reveals the existence of GO in the nanocomposite. The above results indicate that effective combination between GO and TiO_2 nanoparticles are achieved in the present work.

3.2. Spectroscopic analyses

Raman spectrum is considered as an efficient tool for the characterization of carbon materials. As shown in Fig. 3, GO–TiO_2 presents D-band at 1360 cm^{-1} due to first-order zone boundary phonons, and G-band at 1597 cm^{-1} caused by the in-plane optical vibration of GO [24]. The D-band suggests there are defects within the hexagonal graphitic structure, and its intensity decreases in the nanocomposite. The obvious decrease in the D/G intensity ratio after combining with TiO_2 indicates an inducing crystallization, which leads to fewer defects during hydrothermal process [25]. Moreover, the peaks around 146, 397, 516 and 639 cm^{-1} ascribable to anatase TiO_2 show a decreasing trend after combining with GO [26].

Fig. 4a shows the XPS full spectrum of 2 wt% GO–TiO_2. The bands located at binding energies of 464.5 and 458.6 eV can be assigned to $Ti2p_{1/2}$ and $Ti2p_{3/2}$ spin-orbital splitting photo-electrons in the Ti^{4+} chemical state, respectively [27]. The high-resolution spectrum of C1s for the nanocomposite in Fig. 4b is fitted by using XPSPEAK41 software and shirley-type background. The deconvoluted peaks

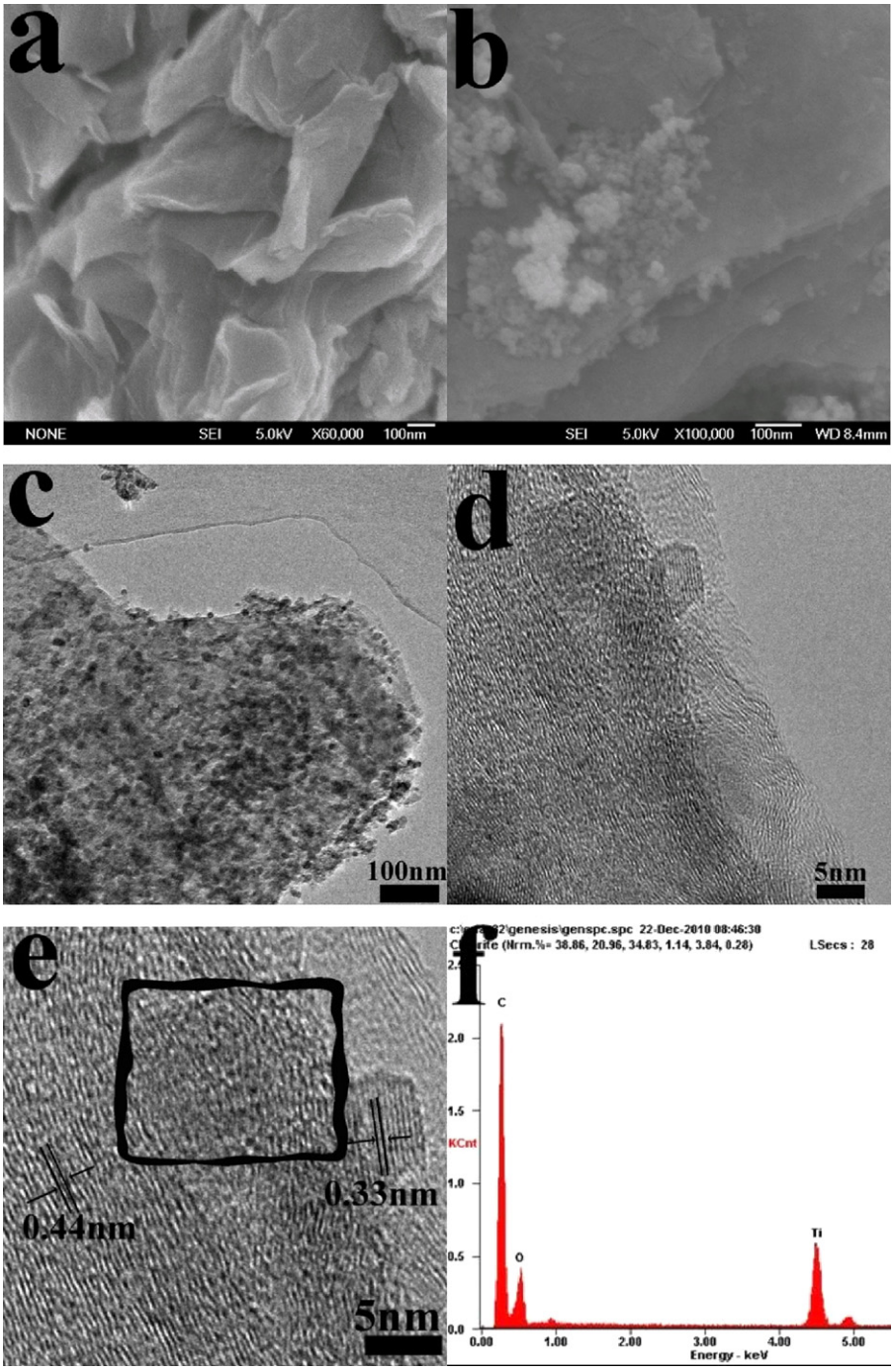

Fig. 2. SEM images of GO (a) and GO–TiO_2 (b), HRTEM images of GO–TiO_2 (c–e), and EDS spectrum (f) of the rectangle region in image e.

centered at the binding energy of 284.8, 285.0, 286.0 and 289.5 eV are attributed to the C—C, C—H, C—OH and O—C=O, respectively [28]. It is known that GO is composed of small aromatic conjugated domains modified with carboxylic, hydroxyl, and epoxide groups [29]. Therefore, the above results confirm that GO is retained some oxidative degree after the hydrothermal process.

Fig. 5 depicts the DRS of the obtained samples. GO shows an absorption spectrum obviously different from G, and the pristine TiO_2 shows the characteristic spectrum with its fundamental absorption edge rising at 400 nm. It is notable that the absorption onset experiences a slight red-shift and an obviously enhanced intensity after the introduction of GO, which is consistent with previous reports [15,30]. Moreover, absorption intensity increases with enhancing the GO content, suggesting that GO can expand the visible light absorption, and modify the fundamental process of photogenerated carrier formation in the nanocomposite.

3.3. *Photocatalytic H_2 evolution efficiency*

As displayed in Fig. 6, photocatalytic H_2 generation can be observed over all catalysts with different GO contents. It could be attributed to the versatile electronic structure of GO [31–33], which results in the photogenerated electrons easily transported to the composite surface and reacted with proton on the active sites. Generally, photocatalyst without co-catalyst loading shows relatively low H_2 production efficiency. Therefore, the effect of Pt-loading

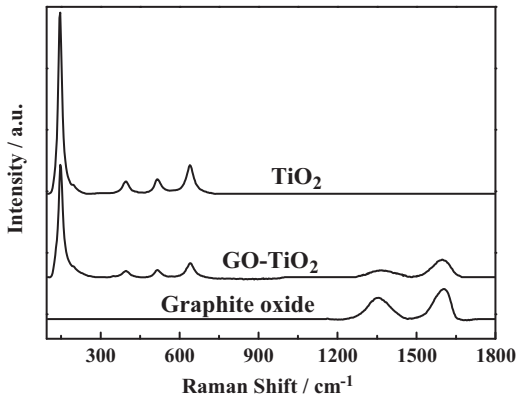

Fig. 3. Raman spectra of GO, TiO_2 and GO–TiO_2.

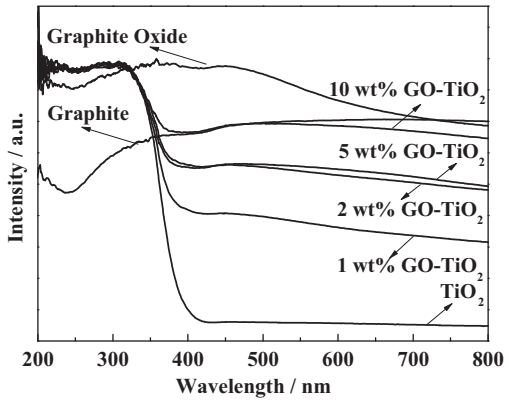

Fig. 5. UV–vis DRS of G and GO–TiO_2 with different GO contents.

amount on the photocatalytic efficiency was investigated. As can be seen from Fig. 7, the increased H_2 evolution rate with enhancing the Pt-loading amount from 0.5 wt% to 2 wt% could be attributed to the formation of Schottky barriers, which is beneficial for the photogenerated carrier separation. In addition, excessive Pt-loading would result in the growth and agglomeration of Pt nanoparticles, which in turn suppress the above basic functions of co-catalyst [34]. Therefore, 2 wt% GO–TiO_2 with 1 wt% Pt-loading gives a maximum H_2 evolution rate of 380 μmol h^{-1}, once the GO content is further increased to 10 wt%, the photoactivity decreased. The reason may be that the excessive GO in composite effectively blocks the TiO_2 excitation since it will shade the incident light. Moreover, it is interesting to find that the pre-irradiation of Hg-lamp can also lead to an enhancement in the photoactivity of GO–TiO_2 without Pt-loading, indicating that GO electrical properties are possibly changed during the photo-deposited process.

The photocatalytic H_2 production rates of the pristine G, GO, TiO_2 and their nanocomposites under different light source irradiation are shown in Table 1. As can be seen, the pristine TiO_2 and G demonstrate no appreciable H_2 evolution under the visible light illumination, and GO shows limited photoactivity for H_2 production under the same condition. Under the full spectra irradiation, GO–TiO_2 and G–TiO_2 exhibit H_2 generation rate of 82.2 μmol h^{-1} and 19.5 μmol h^{-1}, respectively. TiO_2, GO–TiO_2 and G–TiO_2 all show superior photoactivities when 1 wt% Pt-loading, and GO–TiO_2 reaches the maximum H_2 generation rate of 853 μmol h^{-1}, whereas the physical mixture of GO and TiO_2 shows no photoactivity. These phenomena indicate that the simple contact as the case of the mixture of GO and TiO_2 would not lead to the visible-light-driven photoactivity as the photoinduced electrons on GO could not transfer to TiO_2 nanoparticles directly unless a tight contact was formed.

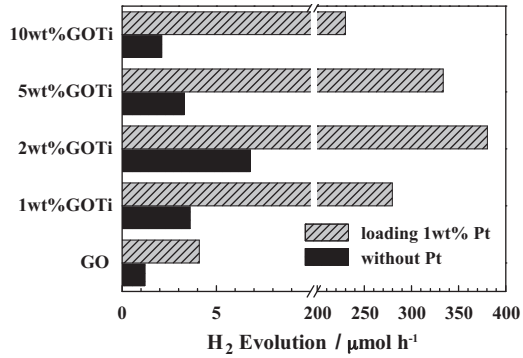

Fig. 6. H_2 evolution rates over GO and GO–TiO_2 containing different GO contents. Condition: 100 mg photocatalysts in 100 mL 10 vol% TEOA solution, 300 W Xe-lamp equipped with cut-off filter (λ ≥ 420 nm), irradiation 2 h.

Therefore, it could be concluded that a good combination between GO and TiO_2 is a crucial factor for the visible-light-driven photoactivity of the nanocomposite, and the present GO–TiO_2 possesses a good combination which is possibly related to the preparation method used. Fig. 8 shows a typical time course for H_2 evolution from 1 wt% Pt-loaded photocatalyst suspension containing 10 vol% TEOA under visible light irradiation. The total H_2 evolution amount over 2 wt% GO–TiO_2 after 10 h is more than 3800 μmol. The apparent quantum yield (AQY) measurements for 2 wt% GO–TiO_2 show a wide photoresponse under monochromatic light wavelength ranged from 350 to 550 nm. The AQY under 420, 475, 520, and 550 nm monochromatic light irradiation is *ca.* 8.2%, 4.3%, 0.4% and 0.5%, respectively.

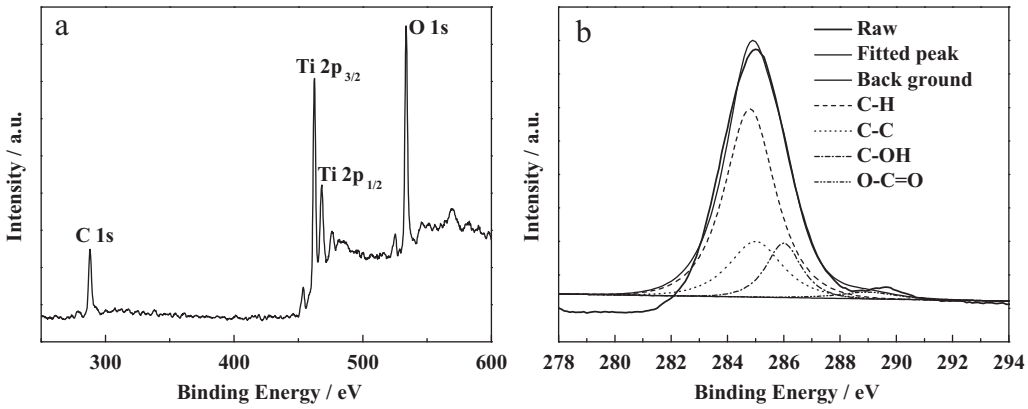

Fig. 4. XPS full spectrum (a) of the GO–TiO_2 and the peak deconvolution (b) of C1s XPS high resolution spectrum.

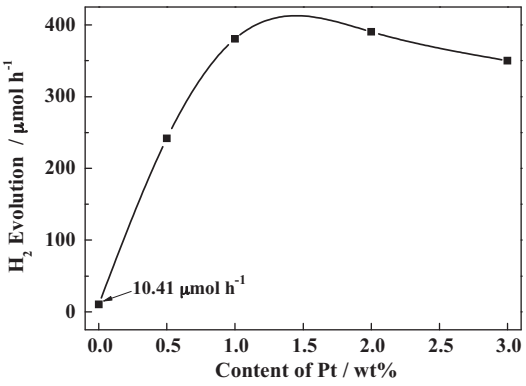

Fig. 7. Effect of the Pt-loading amount on the photocatalytic H_2 production rate. Conditions: 100 mg photocatalysts in 100 mL 10 vol% TEOA solution, 300 W Xe-lamp equipped with a cut-off filter ($\lambda \geq 420$ nm), irradiation 2 h.

Table 1
Photocatalytic activities of various products for H_2 evolution under visible or full spectra irradiation of Xe-lamp.[a]

Material	Hydrogen evolution rate/μmol h^{-1}	
	Visible light	Full spectra
Graphite (G)	0	0
Graphite oxide (GO)	1.2	1.6
Pt/G	0	0
Pt/GO	4.1	4.8
Pt/TiO_2	0	730
G–TiO_2	0	19.5
Pt/(G–TiO_2)	71.5	751
GO–TiO_2	6.8	82.2
Pt/(GO–TiO_2)	380	853
Pt/(GO + TiO_2)[b]	0	713
Pt/G + TiO_2[c]	0	490
Pt/GO + TiO_2	2.5	533

[a] Reaction condition: 100 mg photocatalyst in 100 mL 10 vol% TEOA solution, and 300 W Xe-lamp irradiation 2 h. If indicated, 2 wt% GO or G was added and 1 wt% Pt was loaded.
[b] Mixture of GO and TiO_2 was firstly prepared, and then was loaded with 1 wt% Pt.
[c] Pt-loaded G was firstly prepared, and then mixed with TiO_2.

3.4. Preliminary discussion of photocatalytic mechanism

It has been reported that the electronic property of GO, as an intermediate state between graphene and graphite, can be modulated depending on its oxidation level [35]. Moreover, GO can be completely reduced into graphene by $NaBH_4$, and then used to prepare graphene–TiO_2 nanocomposite photocatalyst [20]. It

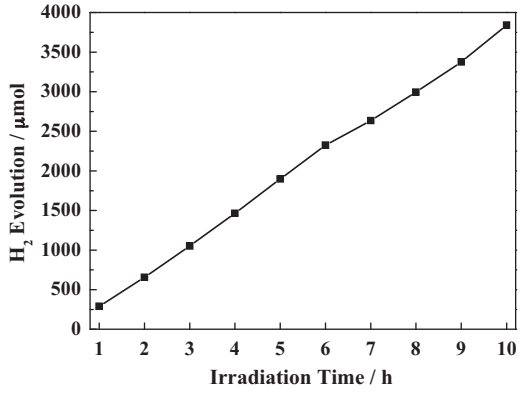

Fig. 8. Typical time course for H_2 evolution over 1 wt% Pt-loaded 2 wt% GO–TiO_2. Conditions: 100 mg photocatalysts in 100 mL 10 vol% TEOA solution, 300 W Xe-lamp equipped with cut-off filter ($\lambda \geq 420$ nm).

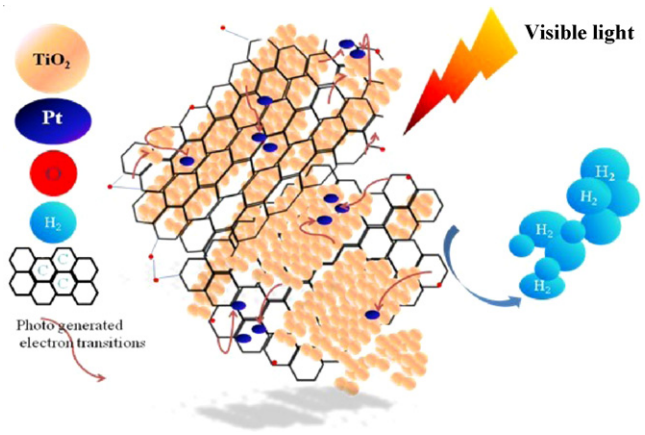

Scheme 1. Schematic diagram of the proposed mechanism for photocatalytic H_2 production over the GO–TiO_2 nanocomposites.

is interesting to find that the G–TiO_2 composite by using a pristine graphite instead of GO as initial carbon source during the hydrothermal process also shows photoactivity. Furthermore, the physical mixture of Pt/GO and TiO_2 (denoted as Pt/GO + TiO_2) shows visible-light-responsive photoactivity, indicating that TiO_2 can be sensitized by the oxidative degree of initial added GO. After the Pt photo-deposition process, photocatalytic H_2 evolution rate shows a remarkable enhancement. This phenomenon could be attributed to the following reasons: (1) Pt particles can act as electron traps and effectively promote H_2 evolution; (2) the present GO could be partly reduced during the photodeposition process and result in reduced bandgap of GO [14], which may be beneficial for photo-generated electrons transferring among the interface of GO–TiO_2 composite. Very recently, visible-light-responsive GO–TiO_2 nanocomposite with p–n heterojunction is reported [36], the same situation might be occurred in the present system. Moreover, it is noteworthy that the physical mixture GO and TiO_2 (denoted as Pt/(GO + TiO_2)) shows almost no photoactivity after the deposition of Pt. The reason might be that the weaken association between GO and TiO_2 could suppress the carriers transition among the interface. Moreover, the pristine TiO_2 could not be excited by visible light, whereas the pristine GO exhibits slight photoactivity for H_2 production.

Based on the above results and discussions, the possible mechanism of photocatalytic activity enhancement under visible light irradiation is proposed in Scheme 1. GO can absorb the visible light and the excited photo-generated electrons (from anti-bonding π^*) are subsequently injected into the conduction band of TiO_2 (d-orbital) due to the d–π interaction. Subsequently, the excited electrons are transferred to the active sites where they reduce the water molecules or proton to produce H_2. The analogous results have been reported in the MWCNTs/TiO_2 systems [13,37].

4. Conclusion

A series of GO–TiO_2 nanocomposite were successfully fabricated though a facile hydrothermal process. The obtained products show highly visible-light-driven photocatalytic activity. 2 wt% GO–TiO_2 shows a maximum H_2 evolution rate of 380 μmol h^{-1} under visible light irradiation and the AQY under 420 nm monochromatic light irradiation is *ca.* 8.2%. An effective combination between GO and TiO_2 achieved by the hydrothermal process is crucial for the visible-light-driven photoactivity for H_2 production, and the GO can serve as photosensitizer in the present GO–TiO_2 system and expand the spectral responsive range of TiO_2 to visible light. The present encouraging results seem to illumine a way to produce hybrids with GO and semiconductor, which may application in the

fields such as photocatalytical reaction, dye-sensitized solar cell, and other photoelectrochemical devices.

Acknowledgements

This work was supported by the NSFC (20973128, 20871096), Program for New Century Excellent Talents in University (NCET-07-0637), and Independence Innovation Program (2081003) of Wuhan University, China. We also gratefully thank Dr. Ying Liu for XPS analysis and helpful discussion.

References

[1] H. Ohkita, S. Cook, Y. Astuti, W. Duffy, S. Tierney, W. Zhang, M. Heeney, I. McCulloch, J. Nelson, D.D.C. Bradley, J.R. Durrant, J. Am. Chem. Soc. 130 (2008) 3030–3042.
[2] K.P. Gong, F. Du, Z.H. Xia, M. Durstock, L.M. Dai, Science 323 (2009) 760–764.
[3] A.K. Geim, K.S. Novoselov, Nat. Mater. 6 (2007) 183–191.
[4] A.K. Geim, Science 324 (2009) 1530–1534.
[5] M.J. McAllister, J.L. Li, D.H. Adamson, H.C. Schniepp, A.A. Abdala, J. Liu, M. Herrera-Alonso, D.L. Milius, R. Car, R.K. Prud'homme, I.A. Aksay, Chem. Mater. 19 (2007) 4396–4404.
[6] R.J.W.E. Lahaye, H.K. Jeong, C.Y. Park, Y.H. Lee, Phys. Rev. B 79 (2009) 125435–125438.
[7] D.R. Dreyer, S. Park, C.W. Bielawski, R.S. Ruoff, Chem. Soc. Rev. 39 (2010) 228–240.
[8] X.B. Chen, S.H. Shen, L.J. Guo, S.S. Mao, Chem. Rev. 110 (2010) 6503–6570.
[9] A. Kudo, Y. Miseki, Chem. Soc. Rev. 38 (2009) 253–278.
[10] Y.F. Lee, K.H. Chang, C.C. Hu, K.M. Lin, J. Mater. Chem. 20 (2010) 5682–5688.
[11] C.X. Pan, H. Yang, J. Alloys Compd. 501 (2010) 8–11.
[12] H.J. Yan, H.X. Yang, J. Alloys Compd. 509 (2011) 26–29.
[13] K. Dai, T.Y. Peng, D.N. Ke, B.Q. Wei, Nanotechnology 20 (2009) 125603–125610.
[14] T.F. Yeh, J.M. Syu, C. Cheng, T.H. Chang, H.S. Teng, Adv. Funct. Mater. 20 (2010) 2255–2262.
[15] H. Zhang, X.J. Lv, Y.M. Li, Y. Wang, J.H. Li, ACS Nano 4 (2010) 380–386.
[16] Y.H. Zhang, Z.R. Tang, X.Z. Fu, Y.J. Xu, ACS Nano 4 (2010) 7303–7314.
[17] J.C. Liu, H.W. Bai, Y.J. Wang, Z.Y. Liu, X.W. Zhang, D.D. Sun, Adv. Funct. Mater. 20 (2010) 4175–4181.
[18] C.Z. Zhu, S.J. Guo, P. Wang, L. Xing, Y.X. Fang, Y.M. Zhai, S.J. Dong, Chem. Commun. 46 (2010) 7148–7150.
[19] Y.Y. Liang, H.L. Wang, H.S. Casalongue, Z. Chen, H.J. Dai, Nano Res. 3 (2010) 701–705.
[20] X.Y. Zhang, H.P. Li, X.L. Cui, Y.H. Lin, J. Mater. Chem. 20 (2010) 2801–2806.
[21] W.S. Hummers, J. Am. Chem. Soc. 80 (1958) 1339.
[22] X.Q. Fu, F.L. Bei, X. Wang, S. O'Brien, J.R. Lombardi, Nanoscale 2 (2010) 1461–1466.
[23] W.G. Su, J. Zhang, Z.C. Feng, T. Chen, P.L. Ying, C. Li, J. Phys. Chem. C 112 (2008) 7710–7716.
[24] Y.W. Zhu, S. Murali, W.W. Cai, X.S. Li, J.W. Suk, J.R. Potts, R.S. Ruoff, Adv. Mater. 22 (2010) 3906–3924.
[25] S. Stankovich, D.A. Dikin, R.D. Piner, K.A. Kohlhaas, A. Kleinhammes, Y. Jia, Y. Wu, S.T. Nguyen, R.S. Ruoff, Carbon 45 (2007) 1558–1565.
[26] H. Wang, Y. Wu, B.Q. Xu, Appl. Catal. B: Environ. 59 (2005) 139–146.
[27] O. Akhavan, E. Ghaderi, J. Phys. Chem. C 113 (2009) 20214–20220.
[28] D. Yang, A. Velamakanni, G. Bozoklu, S. Park, M. Stoller, R.D. Piner, S. Stankovich, I. Jung, D.A. Field, C.A. Ventrice, R.S. Ruoff, Carbon 47 (2009) 145–152.
[29] X.Z. Zhou, X. Huang, X.Y. Qi, S.X. Wu, C. Xue, F.Y.C. Boey, Q.Y. Yan, P. Chen, H. Zhang, J. Phys. Chem. C 113 (2009) 10842–10846.
[30] L.W. Zhang, H.B. Fu, Y.F. Zhu, Adv. Funct. Mater. 18 (2008) 2180–2189.
[31] J.A. Yan, L.D. Xian, M.Y. Chou, Phys. Rev. Lett. 103 (2009) 086802–86806.
[32] Q.H. Zhang, W.Q. Fan, Q.H. Lai, Y. Wang, J. Phys. Chem. C 115 (2011) 10694–10701.
[33] W. Choi, Y. Park, S.H. Kang, Phys. Chem. Chem. Phys. 13 (2011) 9425–9431.
[34] H.B. Yi, T.Y. Peng, D.N. Ke, D. Ke, L. Zan, C.H. Yan, Int. J. Hydrogen Energy 33 (2008) 672–678.
[35] D.W. Boukhvalov, M.I. Katsnelson, J. Am. Chem. Soc. 130 (2008) 10697–10701.
[36] C.C. Che, W.M.M.C. Long, ACS Nano 4 (2010) 6425–6432.
[37] G.M. An, W.H. Ma, Z.Y. Sun, Z.M. Liu, B.X. Han, S.D. Miao, Z.J. Miao, K.L. Ding, Carbon 45 (2007) 1795–1801.